Design and synthesis of bioactive molecules

Edited by Fengzhi Zhang and David R. Spring

Imprint

Synthesis, biological and electrochemical evaluation of glycidyl esters of phosphorus acids as potential anticancer drugs

Almaz A. Zagidullin[*1,2], Emil R. Bulatov[2], Mikhail N. Khrizanforov[3], Damir R. Davletshin[2], Elvina M. Gilyazova[2], Ivan A. Strelkov[1] and Vasily A. Miluykov[1]

Letter

Address:
[1]Arbuzov Institute of Organic and Physical Chemistry, FRC Kazan Scientific Center of Russian Academy of Sciences, Arbuzov Street 8, Kazan, 420088, Russia, [2]Institute of Fundamental Medicine and Biology, Kazan Federal University, Kremlyovskaya Street 18, Kazan, 420008, Russia and [3]Zelinsky Institute of Organic Chemistry, Russian Academy of Sciences, Leninsky prospekt 47, Moscow, 119991, Russia

Email:
Almaz A. Zagidullin[*] - almaz_zagidullin@mail.ru
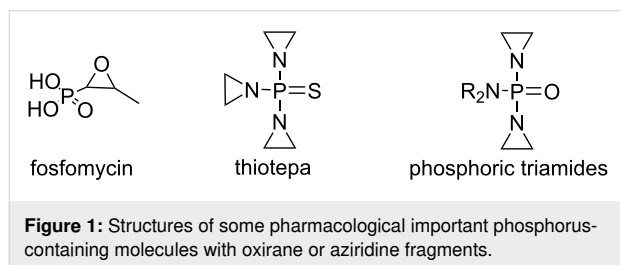
* Corresponding author

Abstract

Organophosphorus compounds are important in synthetic organic chemistry and pharmaceutical applications due to their diverse biological activities. In this study, we synthesized three novel glycidyl esters of phosphorus acids **1–3** via the condensation of chlorophosphine oxides or phosphorus oxychloride with glycidol in the presence of a base, obtaining products with high purity and moderate to excellent yields. Their cytotoxic potential was evaluated using the MTT assay on human fibroblasts (HSF), prostate cancer (PC-3), and breast cancer (MCF7) cell lines, revealing moderate preferential cytotoxicity toward cancer cells, particularly in the case of MCF7. Additionally, linear sweep voltammetry (LSV) studies on human serum albumin (HSA) were conducted to investigate their alkylating properties. The electrochemical results suggest that these compounds effectively modify albumin, highlighting their potential as reactive anticancer agents. These findings provide important insights into the synthesis, cytotoxic activity, and biochemical reactivity of glycidyl esters of phosphorus acids, underscoring their potential as lead structures for further development in anticancer drug discovery and pharmaceutical research.

Introduction

Phosphorus-containing drugs represent a crucial category of therapeutic agents, extensively utilized in clinical practice due to their diverse pharmacological properties and applications [1-4]. These compounds have garnered considerable attention from both pharmaceutical companies and researchers, reflecting their significance in drug development and therapeutic innovation [5-7]. The structural diversity of phosphorus-containing molecules, which includes phosphotriesters, phosphonates, phosphinates, phosphine oxides, and bisphosphonates, allows for tailored modifications that enhance selectivity, bioavailability, and reduce potential side effects [8-13]. This versatility makes them valuable not only as drugs but also as intermediates in synthetic organic chemistry, facilitating access to a wide array of molecular targets [14-16]. The importance of phosphorus-containing drugs extends beyond their therapeutic applications; they also play a pivotal role in addressing specific medical conditions such as chronic kidney disease (CKD) [17,18].

The synthesis of organophosphorus compounds is a dynamic field of research, with numerous synthetic methodologies being explored to create novel phosphorus derivatives [19-21]. Recent studies have highlighted the increasing relevance of three-membered strained cycles containing phosphorus in various domains such as agrochemicals, synthetic chemistry, and medicine. This surge in interest has led to the development of innovative synthetic routes aimed at producing new members of these compounds [22]. For instance, fosfomycin [23] stands out as a broad-spectrum antibiotic currently employed in clinical settings, while thiotepa has been approved for treating several cancers, including gastrointestinal tumors and bladder cancer (Figure 1). Additionally, phosphoric triamides alkylating agents featuring aziridine rings are recognized for their role as nitrogen mustards in cancer therapy [24].

Figure 1: Structures of some pharmacological important phosphorus-containing molecules with oxirane or aziridine fragments.

Although there are numerous examples in the chemical literature regarding the biological activity (including anticancer properties) of phosphoric esters, reports on biological studies of systems based on the P=O fragment and oxirane skeletons are less common. Nevertheless, systems containing both of the mentioned structural motifs are rarely encountered in the literature. In this paper, we report the synthesis, biological activity, and electrochemical evaluation of glycidyl esters of phosphorus acids.

Results and Discussion
Synthesis of glycidyl esters of phosphorus acids **1–3**

Glycidyl esters of phosphorus acids **1–3** were obtained by condensation of chlorophosphine oxides (methylphosphonic dichloride MeP(O)Cl$_2$; methyl dichlorophosphate (MeO)P(O)Cl$_2$) and phosphorus oxychloride P(O)Cl$_3$ with racemic glycidol in CH$_2$Cl$_2$ in the presence of KOH as basic agent (Scheme 1). Further filtration and final distillation at low pressure leads to the products as thick liquids with good yields (44–67%) and purity.
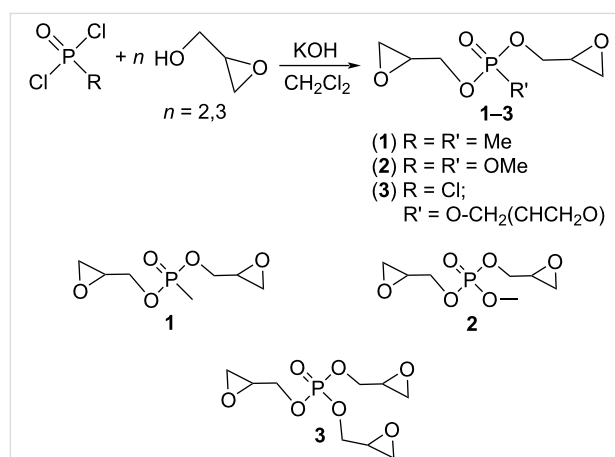
Scheme 1: Synthesis of glycidyl esters of phosphorus acids **1–3**.

The structures of glycidyl esters of phosphorus acids **1–3** were confirmed by ^{31}P, ^{1}H NMR, IR spectroscopy, and elemental analysis (see Experimental part for additional information). The ^{31}P{^{1}H} NMR spectrum of diglycidyl methylphosphonate (**1**) shows a singlet at +32 ppm; for diglycidyl methylphosphate (**2**) and triglycidyl phosphate (**3**) also a singlet in the region 0–1 ppm is observed, despite the presence of a chiral carbon atom in the oxirane fragment. In the ^{1}H NMR spectra of esters **1–3** the characteristic signals of the oxirane fragment at 2.41–3.24 ppm and the POCH$_2$- fragment at 3.66–4.36 ppm can be observed. The NMR data for the glycidyl esters of phosphorus acids **1–3** are comparable to those of related compounds.

Biological activity of glycidyl esters of phosphorus acids

To evaluate the biological activity of diastereomeric mixtures of glycidyl esters of phosphorus acids **1–3**, their cytotoxic effects

were assessed using the MTT assay on two tumor cell lines (PC-3 and MCF7) and one non-cancerous line (HSF). The assay measures the concentration of each compound required to inhibit cellular metabolic activity by 50% (IC$_{50}$). All experiments were performed in biological triplicates, and standard deviations were calculated to assess statistical reliability. The results are summarized in Figure 2 and Table 1.

Table 1: IC$_{50}$ values (µM ± SD) for glycidyl esters of phosphorus acids **1–3** in human skin fibroblasts (HSF), prostate cancer cells (PC-3), and breast cancer cells (MCF7).[a]

Cell line	IC50 (µM)		
	1	**2**	**3**
HSF	394 ± 28	398 ± 33	254 ± 19
PC-3	355 ± 25	300 ± 21	257 ± 20
MCF7	216 ± 16	128 ± 10	182 ± 14

[a]Values represent the mean ± standard deviation (*n* = 3) of biological replicates, determined by MTT assay after 48 hours of treatment. IC$_{50}$ indicates the concentration required to reduce cell viability by 50%; lower values correspond to higher cytotoxic potency.

Diglycidyl methylphosphonate (**1**) reduced cell viability by 50% at concentrations of 394 ± 28 µM, 355 ± 25 µM, and 216 ± 16 µM for HSF, PC-3, and MCF7 cell lines, respectively. Similarly, diglycidyl methylphosphate (**2**) achieved 50% inhibition at concentrations of 398 ± 33 µM, 300 ± 21 µM, and 128 ± 10 µM. Triglycidyl phosphate (**3**) exhibited IC$_{50}$ values of 254 ± 19 µM for HSF, 257 ± 20 µM for PC-3, and 182 ± 14 µM for MCF7 cells.

Among the tested compounds, triglycidyl phosphate (**3**) demonstrated the highest overall cytotoxicity against HSF and PC-3 cell lines, while diglycidyl methylphosphate (**2**) showed the greatest potency toward MCF7 breast cancer cells. Although the IC$_{50}$ values for compounds **1** and **2** were somewhat higher in normal fibroblasts (HSF) compared to cancer cells, the differences were moderate (less than twofold). These results suggest a modest preferential cytotoxicity toward cancer cells, particularly in the case of compound **2** against MCF7, though further studies are needed to establish meaningful selectivity.

Electrochemical studies
Alkylating agents are widely recognized for their ability to form covalent bonds with biological macromolecules (proteins, DNA). The literature discusses the interaction of small molecules with proteins, highlighting how linear sweep voltammetry (LSV) can be used to understand these interactions. The method provides insight into protein structures and functions using electrochemical methods that can also be applied to studies involving alkylating agents [25,26]. In this study, LSV was employed to investigate the interactions between human serum albumin (HSA) and the three prospective alkylating agents **1–3**. The motivation behind these experiments was to explore whether these compounds, which individually exhibit no appreciable redox activity in the potential window applied, can chemically modify (alkylate) serum albumin and thus suppress its characteristic oxidation peaks.

Human serum albumin was chosen as a model protein because of its well-characterized structure and the presence of reactive sites that are known to be susceptible to alkylation. In standard
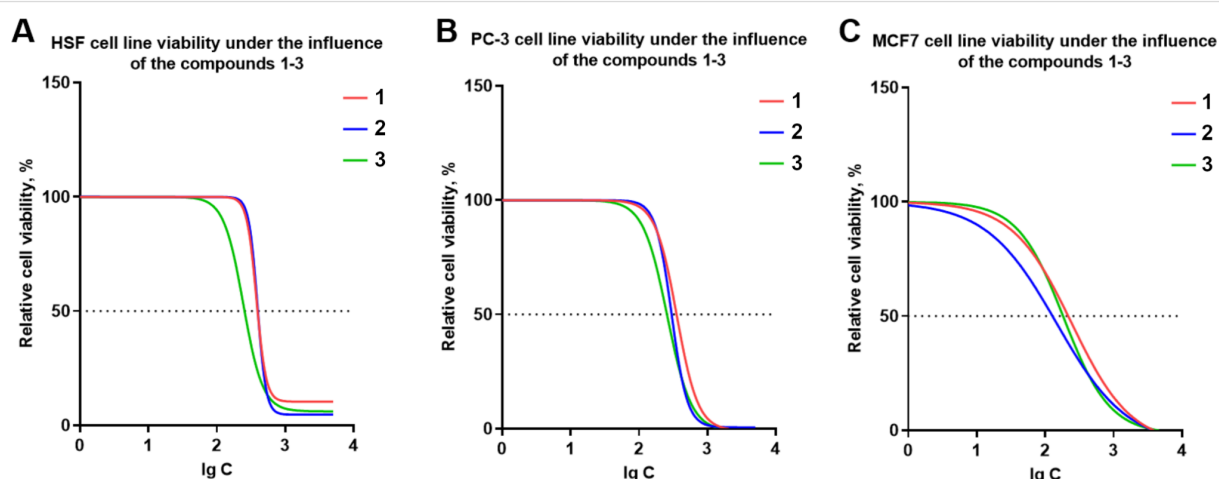

Figure 2: Dose–response curves for the cytotoxic effects of glycidyl esters of phosphorus acids **1–3** on human cell lines. (A) Human skin fibroblasts (HSF), (B) prostate cancer cells (PC-3), and (C) breast cancer cells (MCF7) were treated with diglycidyl methylphosphonate (**1**, red), diglycidyl methylphosphate (**2**, blue), and triglycidyl phosphate (**3**, green) for 48 hours. Cell viability was determined using the MTT assay. Data represent mean ± standard deviation (*n* = 3). The *y*-axis shows relative cell viability (%) compared to untreated control, and the *x*-axis indicates the logarithmic concentration of each compound. The dashed line marks the 50% viability threshold (IC$_{50}$).

aqueous media, the electrochemical oxidation of HSA can be observed via LSV as a broad wave, which is often attributed to the oxidation of amide and other amino acid side-chain fragments. By tracking changes in this oxidation signal upon addition of an alkylating agent, we can infer whether the agent has effectively reacted with (and thus structurally altered) the protein.

As illustrated by the black trace in the LSV plot, pure HSA in aqueous medium shows a characteristic oxidation wave that begins to rise around +0.5 V and significantly increases up to +1.2 V vs Ag/AgCl (Figure 3). This wave is attributed to oxidation processes at peptide bonds or specific side chains (such as cysteine, methionine, tyrosine, serine, tryptophan residues), as well as the overall structure of the protein. The peak intensity and shape can vary depending on pH, ionic strength, and protein conformation. However, under our conditions, the HSA oxidation was consistent, well-defined, and served as a clear baseline reference.
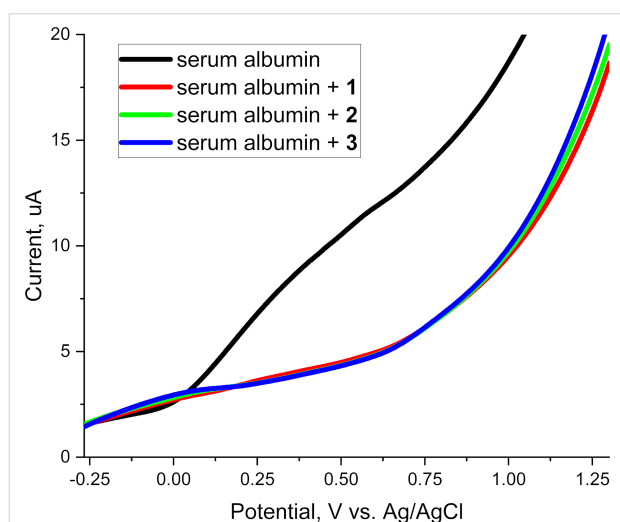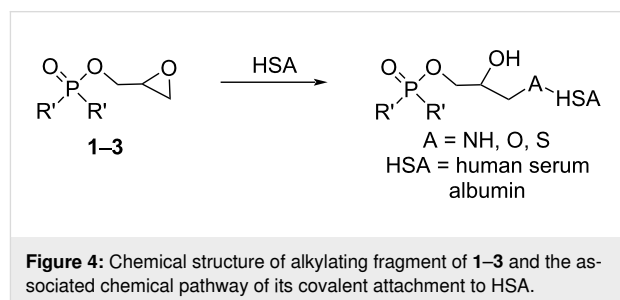

Figure 3: Linear sweep voltammograms of 1×10^{-4} M HSA (black) and HSA mixed with each of the three alkylating agents; **1** (red), **2** (green), and **3** (blue). Conditions: supporting electrolyte: 0.1 M Et$_4$NBF$_4$, working electrode: glassy carbon, scan rate: 0.1 V/s, pH 6.7.

Subsequent to acquiring the control LSV of HSA, 10 µL of each alkylating agent was introduced separately into the albumin solution. As soon as the alkylating agent was added, the characteristic oxidation wave of the albumin nearly vanished or became drastically reduced. Control experiments confirmed that compounds **1–3** themselves exhibit no discernible redox activity in this potential range when tested in the absence of HSA. Consequently, any changes in the recorded voltammogram could be attributed to the interaction (alkylation) of albumin rather than to new electrochemical processes arising directly from the compounds.

When these agents alkylate the HSA amino acid residues (particularly reactive sites like lysine, cysteine, serine NH$_2$, SH, OH-side chains, and possibly other nucleophilic groups), the resulting covalent modification can disrupt the electroactive centers responsible for the protein's oxidation peaks (Figure 4). In many alkylation scenarios, crosslinking or other structural rearrangements can render previously oxidizable moieties inaccessible or shift the protein's conformational state. This suppresses or altogether eliminates the characteristic oxidation wave of HSA.

Figure 4: Chemical structure of alkylating fragment of **1–3** and the associated chemical pathway of its covalent attachment to HSA.

Based on established literature, the significant suppression or disappearance of the HSA oxidation peak upon addition of glycidyl esters **1–3** can be interpreted as evidence of covalent modification (alkylating) of nucleophilic sites on HSA, rather than non-specific binding or merely non-reactive association [27-29]. The observed disappearance of the albumin oxidation peak strongly suggests that all three investigated compounds can modify proteins under physiological conditions. Moreover, the fact that each agent was capable of this disruption aligns well with prior tests on the studied cell lines (PC-3, MCF-7, and HSF), where differences in IC$_{50}$ values reflected the degree of alkylating potency and the selective toxicity toward cancer cells.

Conclusion

In this study, we synthesized and comprehensively characterized a series of glycidyl esters of phosphorus acids **1–3**, evaluating their structural features, cytotoxic potential, and electrochemical behavior. The compounds were efficiently obtained via the condensation of chlorophosphine oxides and phosphorus oxychloride with glycidol, affording high-purity products in moderate to good yields. Cytotoxicity studies revealed that all three compounds possess antiproliferative activity against cancer cell lines (PC-3 and MCF7), with diglycidyl methylphosphate (**2**) demonstrating the highest potency toward MCF7 cells. While all compounds exhibited some level of toxicity toward non-cancerous HSF cells, their IC$_{50}$ values in fibroblasts were generally higher than those observed in tumor cells, indicating a trend toward moderate preferential cytotoxicity. These findings suggest that the glycidyl phosphorus esters,

particularly compound **2**, may serve as promising lead structures for further exploration as anticancer agents.

A key innovation in this work was the application of linear sweep voltammetry (LSV) to investigate the alkylating properties of the synthesized compounds. Unlike traditional biochemical assays, this electrochemical approach enabled real-time monitoring of protein modifications. The significant suppression of human serum albumin (HSA) oxidation peaks following exposure to compounds **1–3** strongly indicates their ability to covalently modify nucleophilic sites in proteins. This finding underscores the potential of LSV as a rapid and effective tool for assessing alkylating reactivity, with implications for future drug development.

Overall, this study offers meaningful insights into the synthesis, cytotoxic behavior, and biochemical reactivity of glycidyl esters of phosphorus acids. The results support their potential as reactive anticancer candidates and lay a foundation for future structure–activity relationship studies and further development in medicinal chemistry.

Experimental

General. All reactions and manipulations were carried out under dry pure N_2 in standard Schlenk apparatus. All solvents were distilled from sodium/benzophenone or phosphorus pentoxide and stored under nitrogen before use. The NMR spectra were recorded on a Bruker MSL-400 (^{1}H 400 MHz, ^{31}P 161.7 MHz, ^{13}C 100.6 MHz). ^{1}H and ^{13}C NMR data are reported with reference to solvent resonances, and ^{31}P NMR spectra were reported with respect to external 85% H_3PO_4 (0 ppm). All experiments were carried out using standard Bruker pulse programs. Infrared (IR) spectra were recorded on a Bruker Vector-22 spectrometer. The elemental analyses were carried out at the microanalysis laboratory of the Arbuzov Institute of Organic and Physical Chemistry, Russian Academy of Sciences.

Cell cultivation. Adherent cell lines HSF (human skin fibroblasts), MCF7 (breast adenocarcinoma), and PC-3 (prostate cancer) were maintained in Dulbecco's Modified Eagle Medium (DMEM) supplemented with 5% fetal bovine serum (FBS), 1 mM L-glutamine, and antibiotics (penicillin 5,000 U/mL and streptomycin 5,000 µg/mL). Cells were incubated at 37 °C in a humidified atmosphere with 5% CO_2. For cytotoxicity assays, cells were seeded into 96-well flat-bottom plates at a density of 5×10^3 cells per well and allowed to adhere for 24 hours under standard culture conditions.

Preparation of compound solutions. Stock solutions of diglycidyl methylphosphonate (**1**), diglycidyl methylphosphate (**2**), and triglycidyl phosphate (**3**) were prepared by dissolving the compounds in the culture medium to a final concentration of 25 mM. These stock solutions were stored and used for subsequent treatments.

Cell treatment. 24 hours after seeding, cells were treated with the test compounds at final concentrations of 25 µM, 50 µM, 100 µM, 250 µM, 500 µM, 750 µM, 1,000 µM, 2,500 µM, and 5,000 µM. Each concentration was tested in triplicate. Control wells received an equivalent volume of culture medium without compounds and served as untreated negative controls.

Cytotoxicity analysis of compounds. After 48 hours of treatment, MTT reagent was added to each well at a final concentration of 0.5 mg/mL. Plates were incubated for 3 hours at 37 °C in a CO_2 incubator to allow for formazan crystal formation. Subsequently, 150 µL of dimethyl sulfoxide (DMSO) was added to each well to solubilize the formazan. Plates were shaken for 15 minutes, and absorbance was measured at 590 nm using an Infinite M200 microplate reader (Tecan, Switzerland). Cell viability was calculated relative to the untreated control (set at 100%). Data were processed and analyzed using GraphPad Prism 10 software.

Electrochemistry. Linear sweep voltammograms were recorded using a BASi Epsilon Eclipse potentiostat (USA). The device includes a measuring unit, a DellOptiplex 320 personal computer with Epsilon-EC-USB-V200 software. As supporting electrolyte 0.1 M Et_4NBF_4 was used. A glassy carbon electrode modified with carbon paste (surface area 1 mm^2) served as the working electrode. Ag/AgCl (0.01 M KCl) was used as a reference electrode. A platinum wire was used as an auxiliary electrode. The scanning rate was 100 mV s^{-1}. Measurements were carried out in a thermostatted electrochemical cell (volume 5 mL) in an inert gas atmosphere (N_2). Between measurements or before recording the voltammetric wave, the aqueous solution was actively stirred with a magnetic stirrer in an atmosphere of constant inert gas flow.

Starting materials. Methylphosphonic dichloride MeP(O)Cl$_2$ and methyl dichlorophosphate (MeO)P(O)Cl$_2$) [30] were prepared according to literature procedures. Phosphorus oxychloride P(O)Cl$_3$ and glycidol were purchased from suppliers and used without additional purification.

Synthesis of diglycidyl methylphosphonate (1). A 500 mL flask with 200 mL of dichloromethane, equipped with a mechanical stirrer, was cooled to −30 °C. Then, 2 equiv of glycidol (21.4 g, 0.289 mol) and 4.2 equiv of potassium hydroxide (34.0 g, 0.607 mol) were added to the flask. Methylphosphonic dichloride MeP(O)Cl$_2$ (1 equiv, 19.2 g, 0.144 mol) was added

dropwise to the mixture with constant stirring in 1 hour. The reaction mixture was additionally stirred at −25 to −30 °C for 2 h and precipitating for 12 h, while the temperature did not rise above 0 °C. After removal of the precipitate by filtration at 25 °C (filter consisted of layers of Celite, sodium sulfate and activated carbon), the filtrate was evaporated under reduced pressure to remove dichloromethane and excess glycidol. After vacuum distillation ($p = 1 \cdot 10^{-3}$ mbar, bp = 130–136 °C) the product diglycidyl methylphosphonate (**1**) was obtained as a thick liquid in 58% yield (17.5 g). ^{1}H NMR (CDCl$_3$, δ, ppm, *J*, Hz) 1.31 (d, $^2J_{PH}$ = 17.8, 3H, Me), 2.41–2.43 (m, 2H, CH$_2$-oxirane), 2.58–2.61 (m, 2H, CH$_2$-oxirane), 2.96–2.98 (m, 2H, CH-oxirane), 3.66–3.69 (m, 2H, OCH$_2$), 4.07–4.09 (m, 2H, OCH$_2$); ^{31}P{^{1}H} NMR (CDCl$_3$, δ, ppm, *J*, Hz) 32.04 (s); IR (liquid, cm^{-1}): 762 (m, oxirane), 858 (m,oxirane), 927 (m, oxirane), 1019 (m), 1139 (w), 1166 (w, P=O), 1240 (m, oxirane), 1316 (m, R-P(O)OR), 1349 (s, P=O), 1425 (w), 1455 (m), 1647 (m), 2932 (m), 3004 (m), 3066 (w); Anal. calcd for C$_7$H$_{13}$PO$_5$: C, 40.39; H, 6.30; O, 38.43; P, 14.88; found: C, 40.24; H, 6.52; P, 14.79.

Synthesis of diglycidyl methylphosphate (2). A 500 mL flask with 200 mL of dichloromethane, equipped with a mechanical stirrer, was cooled to −30 °C. Then, 2 equiv of glycidol (20.0 g, 0.27 mol) and 4.2 equiv of potassium hydroxide (31.8 g, 0.567 mol) were added to the flask. Methyl dichlorophosphate (MeO)P(O)Cl$_2$ (1 equiv, 20.1 g, 0.135 mol) was added dropwise to the mixture with constant stirring in 1 hour. The reaction mixture was additionally stirred at −25 to −30 °C for 2 h and precipitating for 12 h, while the temperature did not rise above 0 °C. After removal of the precipitate by filtration at 25 °C (filter consisted of layers of Celite, sodium sulfate and activated carbon), the filtrate was evaporated under reduced pressure to remove dichloromethane and excess glycidol. After two vacuum distillations ($p = 1 \cdot 10^{-3}$ mbar, bp 113–116 °C) the product diglycidyl methylphosphate (**2**) was obtained as a thick liquid in 44% yield (13.5 g). ^{1}H NMR (CDCl$_3$, δ, ppm, *J*, Hz) 2.49–2.55 (m, 2H, CH$_2$-oxirane), 2.67–2.72 (m, 2H, CH$_2$-oxirane), 3.06–3.14 (m, 2H, CH-oxirane), 3.65 (d, $^3J_{PH}$ = 11.4, 3H, Me), 3.75–3.84 (m, 2H, OCH$_2$), 4.13–4.23 (m, 2H, OCH$_2$); ^{31}P{^{1}H} NMR (CDCl$_3$, δ, ppm, *J*, Hz) −0.1 (s); IR (liquid, cm^{-1}): 598 (w), 763 (m, oxirane), 865 (m, oxirane), 921 (m, oxirane), 1021 (m, P(O)(OR)$_2$), 1140 (w, P(O)(OR)$_2$), 1168 (s, P(O)(OR)$_2$), 1185 (w), 1261 (m), 1350 (m, P=O), 1430 (w), 1455 (m), 1644 (w), 2858 (w), 2960 (w), 3008 (w), 3066 (w); Anal. calcd for C$_7$H$_{13}$PO$_6$: C, 37.51; H, 5.85; O, 42.83; P, 13.82; found: C, 37.50; H, 6.03; P, 13.97.

Synthesis of triglycidyl phosphate (3). Synthesis of **3** was carried out in a manner similar to [31], but without sodium

sulfate as a drying agent. A 500 mL flask with 200 mL of dichloromethane, equipped with a mechanical stirrer, was cooled to −30 °C. Then, 3 equiv of glycidol (22.6 g, 0.305 mol) and 4.5 equiv of potassium hydroxide (25.6 g, 0.457 mol) were added to the flask. Phosphorus oxychloride P(O)Cl$_3$ (1 equiv, 15.6 g, 0.102 mol) was added dropwise to the mixture with constant stirring in 1 hour. The reaction mixture was additionally stirred at −25 to −30 °C for 3 h and precipitating for 12 h, while the temperature did not rise above 10 °C. After removal of the precipitate by filtration at 25 °C (filter consisted of layers of Celite, sodium sulfate and activated carbon), the filtrate was evaporated under reduced pressure to remove dichloromethane and excess glycidol. The product triglycidyl phosphate (**3**) was obtained as a yellowish thick liquid in 67% yield (18.1 g). ^{1}H NMR (CDCl$_3$, δ, ppm, *J*, Hz) 2.56–2.65 (m, 3H, CH$_2$-oxirane), 2.74–2.85 (m, 3H, CH$_2$-oxirane), 3.14–3.24 (m, 3H, CH-oxirane), 3.84–3.95 (m, 3H, OCH$_2$), 4.22–4.36 (m, 3H, OCH$_2$); ^{31}P{^{1}H} NMR (CDCl$_3$, δ, ppm, *J*, Hz) −1.2 (s); IR (liquid, cm^{-1}): 599 (w), 700 (w), 763 (m, oxirane), 797 (m, oxirane), 869 (m, oxirane), 918 (m, oxirane), 1024 (m), 1139 (w, P=O), 1166 (s, P=O), 1259 (m), 1349 (m, P=O), 1429 (w), 1454 (m), 1483 (w), 1520 (w), 1634–1644 (m), 2614 (w), 2899 (w), 2953 (m), 3006 (m), 3065 (m); Anal. calcd for C$_9$H$_{15}$PO$_7$: C, 40.61; H, 5.68; O, 42.07; P, 11.64; found: C, 40.85; H, 5.82; P, 11.97.

Supporting Information

Supporting Information File 1
^{1}H, ^{31}P NMR and IR spectra of compounds **1**–**3**.
[https://www.beilstein-journals.org/bjoc/content/supplementary/1860-5397-21-148-S1.pdf]

Author Contributions

Almaz A. Zagidullin: investigation. Emil R. Bulatov: investigation. Mikhail N. Khrizanforov: investigation. Damir R. Davletshin: investigation. Elvina M. Gilyazova: investigation. Ivan A.

Strelkov: investigation. Vasily A. Miluykov: writing – original draft.

ORCID® iDs

Almaz A. Zagidullin - https://orcid.org/0000-0003-3125-7506
Vasily A. Miluykov - https://orcid.org/0000-0002-8069-457X

Data Availability Statement

All data that supports the findings of this study is available in the published article and/or the supporting information of this article.

References

1. Dormán, G.; Szalai, Z.; Keglevich, G. *ChemMedChem* **2024,** *19,* e202400370. doi:10.1002/cmdc.202400370
2. Finkbeiner, P.; Hehn, J. P.; Gnamm, C. *J. Med. Chem.* **2020,** *63,* 7081–7107. doi:10.1021/acs.jmedchem.0c00407
3. Rodriguez, J. B.; Gallo-Rodriguez, C. *ChemMedChem* **2019,** *14,* 190–216. doi:10.1002/cmdc.201800693
4. Kumar, A.; Mukhopadhyay, J.; Bhagat, S. *ChemistrySelect* **2024,** *9,* e202404258. doi:10.1002/slct.202404258
5. Yu, H.; Yang, H.; Shi, E.; Tang, W. *Med. Drug Discovery* **2020,** *8,* 100063. doi:10.1016/j.medidd.2020.100063
6. Zielonka, J.; Joseph, J.; Sikora, A.; Hardy, M.; Ouari, O.; Vasquez-Vivar, J.; Cheng, G.; Lopez, M.; Kalyanaraman, B. *Chem. Rev.* **2017,** *117,* 10043–10120. doi:10.1021/acs.chemrev.7b00042
7. Pradere, U.; Garnier-Amblard, E. C.; Coats, S. J.; Amblard, F.; Schinazi, R. F. *Chem. Rev.* **2014,** *114,* 9154–9218. doi:10.1021/cr5002035
8. Farrell, R. E.; Steele, H.; Middleton, R. J.; Skropeta, D.; Liu, G.-J. *RSC Med. Chem.* **2024,** *15,* 1973–1981. doi:10.1039/d4md00115j
9. Wu, J.; Xu, R.; Shao, M.; Zhao, L.; Xu, W.; Guo, Y. *ACS Appl. Nano Mater.* **2024,** *7,* 11022–11036. doi:10.1021/acsanm.4c00015
10. Gibadullina, E.; Neganova, M.; Aleksandrova, Y.; Nguyen, H. B. T.; Voloshina, A.; Khrizanforov, M.; Nguyen, T. T.; Vinyukova, E.; Volcho, K.; Tsypyshev, D.; Lyubina, A.; Amerhanova, S.; Strelnik, A.; Voronina, J.; Islamov, D.; Zhapparbergenov, R.; Appazov, N.; Chabuka, B.; Christopher, K.; Burilov, A.; Salakhutdinov, N.; Sinyashin, O.; Alabugin, I. *Int. J. Mol. Sci.* **2023,** *24,* 12637. doi:10.3390/ijms241612637
11. Tsepaeva, O. V.; Nemtarev, A. V.; Pashirova, T. N.; Khokhlachev, M. V.; Lyubina, A. P.; Amerkhanova, S. K.; Voloshina, A. D.; Mironov, V. F. *RSC Med. Chem.* **2023,** *14,* 454–469. doi:10.1039/d2md00363e
12. Ermolaev, V. V.; Arkhipova, D. M.; Miluykov, V. A.; Lyubina, A. P.; Amerhanova, S. K.; Kulik, N. V.; Voloshina, A. D.; Ananikov, V. P. *Int. J. Mol. Sci.* **2021,** *23,* 86. doi:10.3390/ijms23010086
13. Terekhova, N. V.; Lyubina, A. P.; Voloshina, A. D.; Sapunova, A. S.; Khayarov, K. R.; Islamov, D. R.; Usachev, K. S.; Evtugyn, V. G.; Tatarinov, D. A.; Mironov, V. F. *Bioorg. Chem.* **2022,** *127,* 106030. doi:10.1016/j.bioorg.2022.106030
14. Mironov, V. F.; Dimukhametov, M. N.; Nemtarev, A. V.; Pashirova, T. N.; Tsepaeva, O. V.; Voloshina, A. D.; Vyshtakalyuk, A. B.; Litvinov, I. A.; Lyubina, A. P.; Sapunova, A. S.; Abramova, D. F.; Zobov, V. V. *Nanomaterials* **2023,** *13,* 2840. doi:10.3390/nano13212840
15. Pashirova, T. N.; Nemtarev, A. V.; Souto, E. B.; Mironov, V. F. *Russ. Chem. Rev.* **2023,** *92,* RCR5095. doi:10.59761/rcr5095
16. Terekhova, N. V.; Khailova, L. S.; Rokitskaya, T. I.; Nazarov, P. A.; Islamov, D. R.; Usachev, K. S.; Tatarinov, D. A.; Mironov, V. F.; Kotova, E. A.; Antonenko, Y. N. *ACS Omega* **2021,** *6,* 20676–20685. doi:10.1021/acsomega.1c02909
17. Bacchetta, J.; Bernardor, J.; Garnier, C.; Naud, C.; Ranchin, B. *Calcif. Tissue Int.* **2021,** *108,* 116–127. doi:10.1007/s00223-020-00665-8
18. Lobo, L.; Kishore, N.; Sharma, M. *J. Drug Delivery Ther.* **2024,** *14,* 176–181. doi:10.22270/jddt.v14i1.6336
19. Zagidullin, A. A.; Sakhapov, I. F.; Miluykov, V. A.; Yakhvarov, D. G. *Molecules* **2021,** *26,* 5283. doi:10.3390/molecules26175283
20. Oshchepkova, E. S.; Zagidullin, A. A.; Miluykov, V. A.; Sinyashin, O. G. *Phosphorus, Sulfur Silicon Relat. Elem.* **2016,** *191,* 1530–1532. doi:10.1080/10426507.2016.1212350
21. Zagidullin, A.; Ganushevich, Y.; Miluykov, V.; Sinyashin, O.; Hey-Hawkins, E. *Phosphorus, Sulfur Silicon Relat. Elem.* **2013,** *188,* 238–242. doi:10.1080/10426507.2012.744017
22. Mayorquín-Torres, M. C.; Simoens, A.; Bonneure, E.; Stevens, C. V. *Chem. Rev.* **2024,** *124,* 7907–7975. doi:10.1021/acs.chemrev.4c00090
23. Falagas, M. E.; Vouloumanou, E. K.; Samonis, G.; Vardakas, K. Z. *Clin. Microbiol. Rev.* **2016,** *29,* 321–347. doi:10.1128/cmr.00068-15
24. van Maanen, M. J.; Smeets, C. J. M.; Beijnen, J. H. *Cancer Treat. Rev.* **2000,** *26,* 257–268. doi:10.1053/ctrv.2000.0170
25. Parker, V. D.; Roddick, A.; Seefeldt, L. C.; Wang, H.; Zheng, G. *Anal. Biochem.* **1997,** *249,* 212–218. doi:10.1006/abio.1997.2176
26. Sun, W.; Zhao, N.; Niu, X.; Wang, Y.; Jiao, K. *J. Chem. Sci.* **2009,** *121,* 217–223. doi:10.1007/s12039-009-0025-8
27. Zatloukalova, M.; Mojovic, M.; Pavicevic, A.; Kabelac, M.; Freeman, B. A.; Pekarova, M.; Vacek, J. *Redox Biol.* **2019,** *24,* 101213. doi:10.1016/j.redox.2019.101213
28. Attar, A. M.; Richardson, M. B.; Speciale, G.; Majumdar, S.; Dyer, R. P.; Sanders, E. C.; Penner, R. M.; Weiss, G. A. *ACS Appl. Mater. Interfaces* **2019,** *11,* 4757–4765. doi:10.1021/acsami.8b16071
29. Fu, L.; Liu, X.-f.; Zhou, Q.-x.; Zhang, J.-x.; Dong, J.-y.; Wang, J.-f. *J. Lumin.* **2014,** *149,* 208–214. doi:10.1016/j.jlumin.2014.01.023
30. Zagidullin, A. A.; Naileva, F. F.; Fayzullin, R. R.; Islamov, D. R.; Miluykov, V. A. *J. Mol. Struct.* **2025,** *1338,* 142323. doi:10.1016/j.molstruc.2025.142323
31. Amirov, R. R.; Akhmadiev, K.; Gaifutdinov, A. M.; Andrianova, K. A.; Shmelev, A.; Gatiatulin, A. K.; Zagidullin, A. A.; Milyukov, V. A.; Amirova, L. M. *Mater. Today Chem.* **2023,** *29,* 101464. doi:10.1016/j.mtchem.2023.101464

Rhodium-catalysed connective synthesis of diverse reactive probes bearing S(VI) electrophilic warheads

Scott Rice[1,2], Julian Chesti[1,2], William R. T. Mosedale[3], Megan H. Wright[1,2], Stephen P. Marsden[1], Terry K. Smith[3] and Adam Nelson[*1,2]

Full Research Paper

Address:
[1]School of Chemistry, University of Leeds, Leeds, LS2 9JT, UK, [2]Astbury Centre for Structural Molecular Biology, University of Leeds, Leeds, LS2 9JT, UK and [3]Schools of Biology and Chemistry, Biomedical Sciences Research Complex, University of St Andrews, St Andrews, KY16 9ST, UK

Email:
Adam Nelson[*] - a.s.nelson@leeds.ac.uk

* Corresponding author

Keywords:
covalent probes; molecular diversity; rhodium carbenoids

Abstract

The value of small molecules that chemically modify proteins is increasingly being recognised and utilised in both chemical biology and drug discovery. The discovery of such chemical tools may be enabled by screening diverse sets of reactive probes. Most existing sets of reactive probes are armed with cysteine-directed warheads, a limitation that we sought to address. A connective synthesis was developed in which α-diazoamide substrates, armed with a S(VI) warhead, were reacted with diverse co-substrates. A high-throughput approach was used to identify promising substrate/co-substrate/catalyst combinations which were then prioritised for purification by mass-directed HPLC to yield a total of thirty reactive probes. The structural diversity of the probe set was increased by the multiplicity of reaction types between rhodium carbenoids and the many different co-substrate classes, and the catalyst-driven selectivity between these pathways. The probes were screened for activity against *Trypanosma brucei*, and four probes with promising anti-trypanosomal activity were identified. Remarkably, the synthetic approach was compatible with building blocks bearing three different S(VI) warheads, enabling the direct connective synthesis of diverse reactive probes armed with non-cysteine-directed warheads. Reactive probes that are synthetically accessible using our approach may be of value in the discovery of small molecule modifiers for investigating and engineering proteins.

Introduction

Diverse sets of reactive probes can facilitate the discovery of chemical tools and drugs that chemically modify protein targets [1-3]. Established sets of reactive probes are typically armed with electrophilic warheads that have the potential to target nucleophilic amino acid side chains. Most reactive probe sets bear cysteine-directed warheads [3-7], although sets have also been designed to target a wider range of amino acids [8-10]. Sets of reactive probes are generally prepared using robust reac-

tions, most usually amide formation, chosen from the toolkit that currently dominates medicinal chemistry [11] which may, in turn, limit probe structural diversity.

We have developed a unified connective approach for the synthesis of structurally diverse reactive probes bearing S(VI) electrophiles. Proteome-wide screens have shown that S(VI) electrophiles predominantly target lysine and tyrosine [12], although other residues (e.g. serine) may also be targeted within enzyme active sites [13]. It was envisaged that the reactive probes would be prepared by dirhodium-catalysed reactions between pairs of building blocks: an α-diazoamide **2** bearing a S(VI) electrophile and a suitable co-substrate (→ **3**) (Figure 1). Here, metal-catalysed carbenoid chemistry was chosen because of the wide range of potentially reactive functional groups that might be incorporated into co-substrates [14]. The richness of potential connective chemistry, and the availability of alternative dirhodium catalysts with distinctive reactivity, was expected to expand the structural diversity of accessible reactive probes. Herein, we describe the successful execution of this approach and the demonstration of biological function of the resulting reactive probes.

Results and Discussion

We prepared five α-diazoamide substrates bearing S(VI) electrophiles (Scheme 1 and Table 1) [15]. Initially, three amines – morpholine, 4-phenylpiperidine and isoindoline – were reacted with 2,2,6-trimethyl-4*H*-1,3-dioxin-4-one to give the corresponding β-ketoamides **4**. Treatment of the β-ketoamides **4** with 4-acetamidobenzenesulfonyl azide (*p*-ABSA) and triethyl-

amine gave the α-diazo-β-ketoamides **5**. Subsequent KOH-mediated deacetylation yielded the corresponding α-diazo-amides **1**. Finally, Pd-catalysed cross-coupling with warhead-substituted phenyl iodides gave, in low to moderate yield, the required α-diazoamide substrates **2** (referred to individually as **D1**–**5** below). Whilst the Pd-catalysed arylation of α-diazo-amides and esters is known [15-19], its tolerance of pendant S(VI) electrophiles has not been previously explored and is notable.

Due to the relatively large size of the diazo substrates **D1–5**, it was decided to design a set of diverse co-substrates with 15 or fewer heavy (non-hydrogen) atoms. It was decided that the set should include co-substrates with the potential to react with metal carbenoids in many different ways [14], for example through O–H, N–H or formal C–H insertion, cyclopropanation, or oxazole [20] formation. The 16 co-substrates, selected from available compounds in our laboratory, are shown in Figure 2 (panel A). Many of these substrates had more than one potentially reactive site to enable, for example, O–H insertion (**C1–5**, **C8**, **C11** and **C14**), N–H insertion (**C3**, **C6**, **C12**, **C13** and **C15**), formal C–H insertion (**C1**, **C3**, **C4**, **C12**, **C15** and **C16**), oxazole formation (**C9** and **C10**) and cyclopropanation (**C7**, **C10**, **C14** and **C16**).

To start with, we investigated reactions of the α-diazoamide substrates **D1**, **D2** and **D3** with the 16 co-substrates **C1–16** catalysed by three diverse [21] dirhodium catalysts (Rh$_2$piv$_4$, Rh$_2$pfb$_4$ and Rh$_2$cap$_4$) i.e., an array of 144 reactions. An α-diazoamide substrate (20 μmol; 16 μL of a 1.25 M solution in
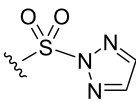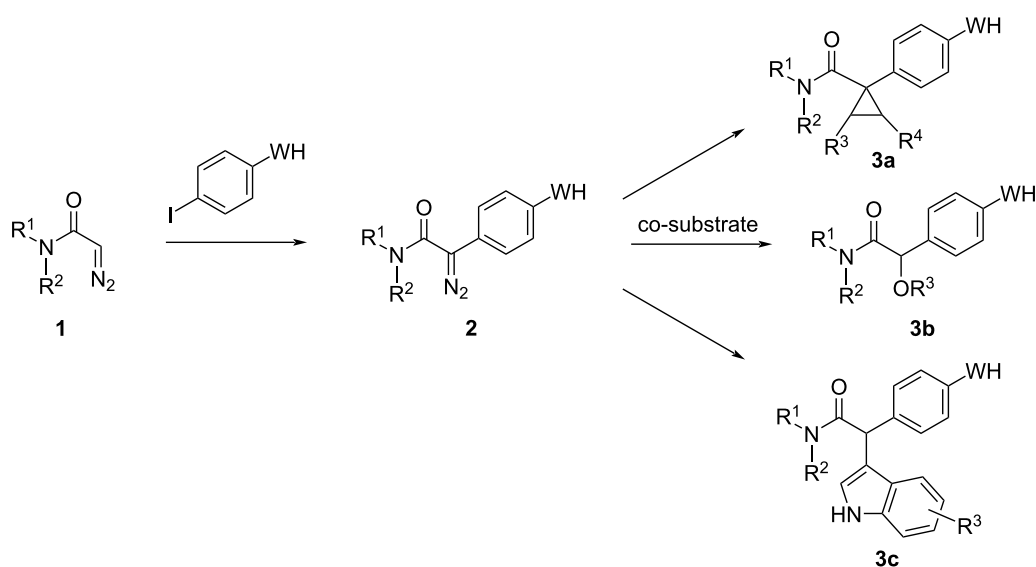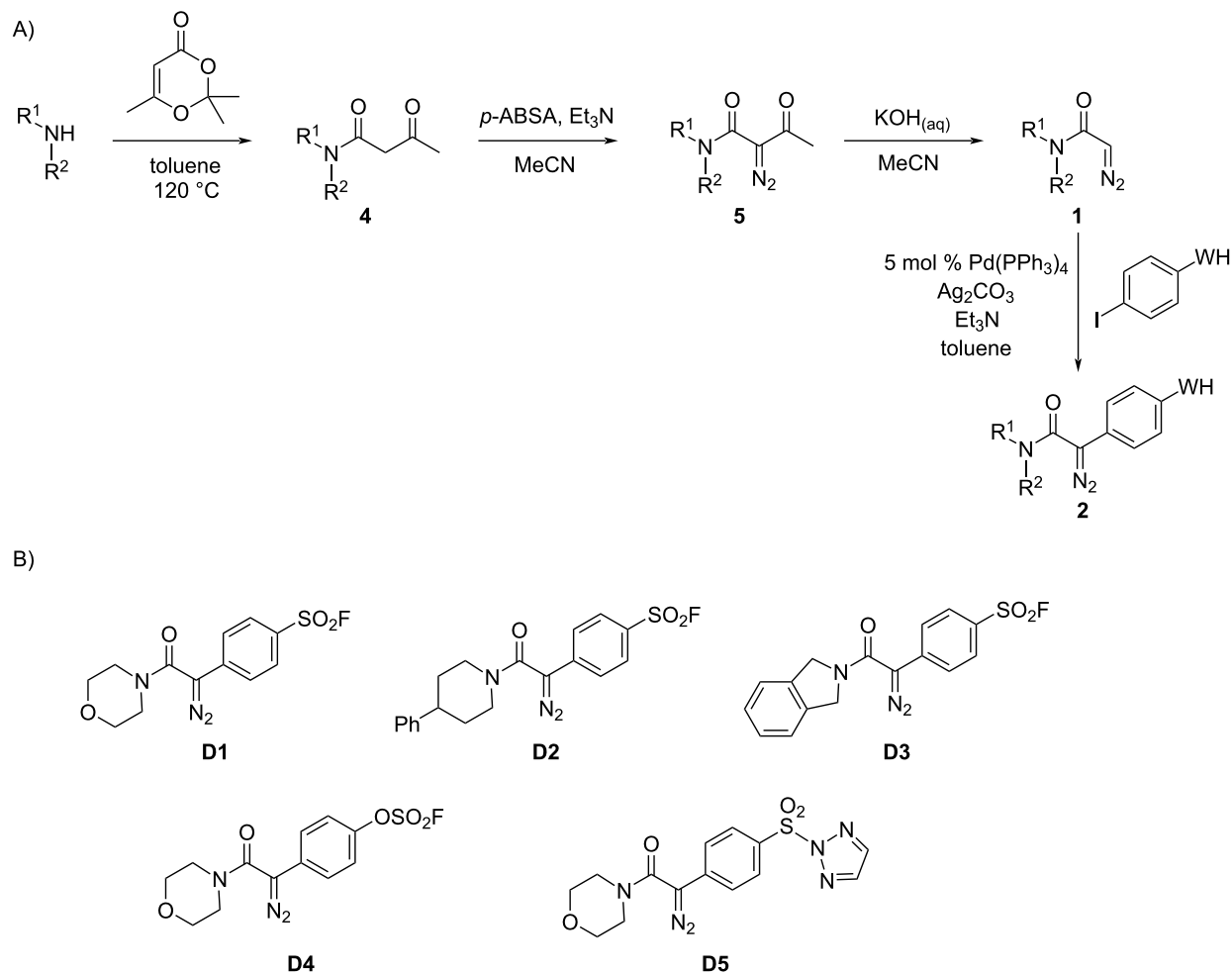

Figure 1: Envisaged connective synthesis of reactive probes **3** bearing S(VI) electrophilic warheads (WH). Diverse probes **3** might be accessible by functionalising α-diazoamide substrates **2** via alternative reaction modes.

Scheme 1: Synthesis of α-diazoamide substrates **D1–5** of general structure **2** bearing S(VI) electrophiles. Panel A: Overview of synthesis (see Table 1 for details of synthesis of individual substrates). Panel B: Substrates that were prepared.

Table 1: Synthesis of α-diazoamide substrates of general structure **2** bearing S(VI) electrophiles (see Scheme 1).

Amine	Yield **4** (%)	Yield **5** (%)	Yield **1** (%)	WH	Substrate (yield, %)
morpholine	94	80	55	–SO$_2$F	**D1** (46)
				–OSO$_2$F	**D4** (26)
				(sulfonyl-triazole)	**D5** (23)
4-phenylpiperidine	85	82	87	–SO$_2$F	**D2** (53)
isoindoline	88	86	99	–SO$_2$F	**D3** (12)

CH$_2$Cl$_2$) and a co-substrate (5 equiv; 16 µL of a 6.25 M solution in CH$_2$Cl$_2$) were added to glass vials in a 96-well reaction block, and the solvent left to evaporate after each addition. Subsequently, a dirhodium catalyst (1 mol %; 200 µL of a 1 mM solution in CH$_2$Cl$_2$) was also added to each vial. The final volume of each reaction was thus 200 µL, with final concentrations of 100 mM (for substrates), 500 mM (for co-substrates) and 1 mM (for catalysts).

A)
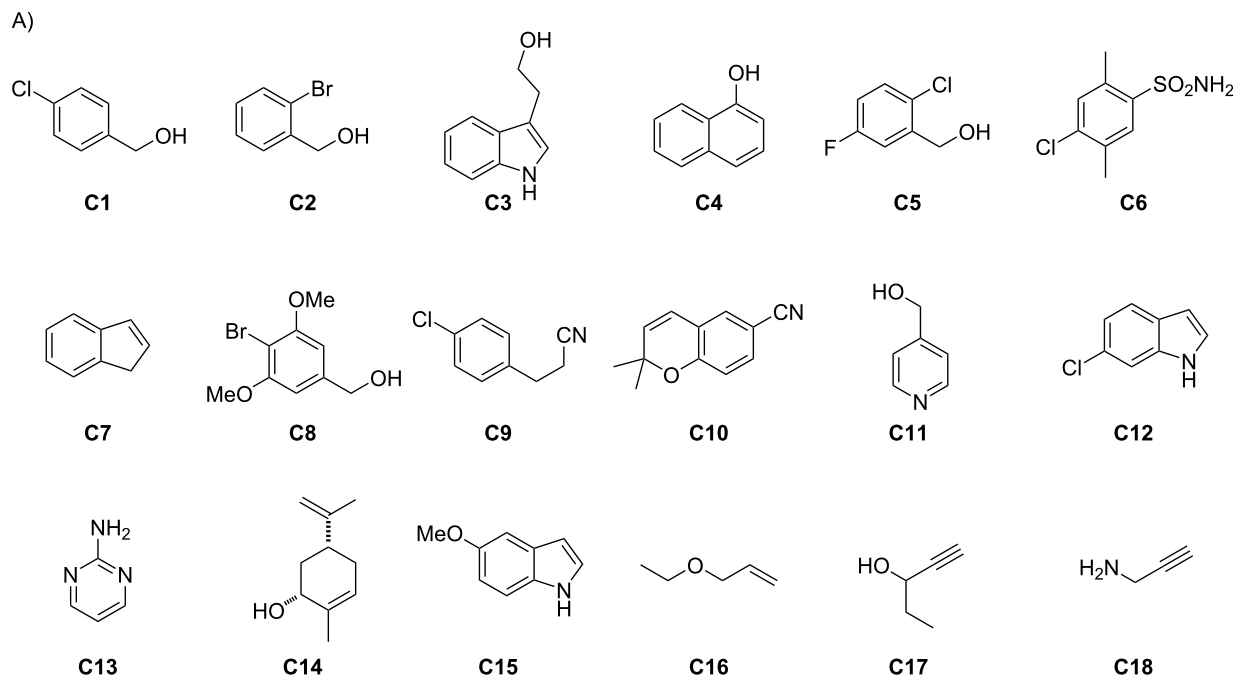
B)

	catalyst	C1	C2	C3	C4	C5	C6	C7	C8	C9	C10	C11	C12	C13	C14	C15	C16
D1	Rh$_2$piv$_4$	8	10	7	2	10	7	–	10	–	–	–	8[a]	9	–	15[a]	–
	Rh$_2$pfb$_4$	12	9	16	8	13	6	–	11	–	–	–	14[a]	–	6	24[a]	–
	Rh$_2$cap$_4$	16	14	10[a]	4	12	9	4	14	–	–	–	3	–	6	10	–
D2	Rh$_2$piv$_4$	10	11	11[a]	2	13	12	12	13	–	–	–	–	12	8	19[a]	–
	Rh$_2$pfb$_4$	18	13	18	13	17	5	7	14	–	–	–	17[a]	–	12	17[a]	–
	Rh$_2$cap$_4$	10	19	14[a]	10	20	13	2	18	–	–	–	4	–	15	15	–
D3	Rh$_2$piv$_4$	5	14	–	9	5	7	–	4	–	–	–	2	9	-	5[a]	–
	Rh$_2$pfb$_4$	3	8	9	8	3	5	–	9	–	–	–	5[a]	–	2	2	–
	Rh$_2$cap$_4$	3	4	7	10	4	2	5	6	–	–	–	3[a]	–	4	10[a]	–

Figure 2: Structures and reactions of co-substrates. Panel A: structures of the 16 selected co-substrates **C1–16**, together with two additional co-substrates **C17** and **C18** that were subsequently used. Panel B: yields, estimated by evaporative light scattering detection, of reactions involving combinations of substrates, co-substrates and catalysts (dash: <2% estimated yield). Highlighted combinations (green boxes) were selected for mass-directed purification. [a]Multiple intermolecular products observed by analytical HPLC.

After 48 h, the outcome of the reactions was determined by analytical UPLC–MS with, additionally, evaporative light-scattering detection [22,23] to enable estimation of the yield of each product (Figure 2, panel B). It was found that many reactions involving alcohol- (e.g., **C1–5**, **C8**, **C11** and **C14**) and indole- (e.g., **C3**, **C12** and **C15**) containing co-substrates yielded intermolecular products, whilst those involving nitrile-containing co-substrates (**C9** and **10**) and the allylic ether **C16** did not. It is remarkable that S(VI) electrophiles are tolerated. Eighteen substrate/co-substrate combinations gave, with at least one of the

catalysts, an intermolecular product in >10% estimated yield (typically corresponding to >1 mg product). For all but one of these reactions, a product with molecular weight consistent with O–H insertion into water was also observed. For these 18 substrate/co-substrate combinations, the reaction with the highest estimated yield was selected for mass-directed purification (Table 2). In total, 23 intermolecular reaction products were isolated and structurally characterised (using, where appropriate, HMBC, COSY and nOe NMR methods; see Figure 3). In general, the yields of these products were rather low, which

Table 2: Outcomes of reactions between α-diazoamide substrates and co-substrates.

Diazo	Co-substrate	Catalyst	Product[a]	Yield[b]
D1	**C1**	Rh_2cap_4	**1-1**	14
D1	**C2**	Rh_2cap_4	**1-2**	12
D1	**C3**	Rh_2pfb_4	**1-3a**	15
			1-3b	1
D1	**C5**	Rh_2pfb_4	**1-5**	11
D1	**C8**	Rh_2cap_4	**1-8**	12
D1	**C15**	Rh_2piv_4	**1-15a**	6
			1-15b	8
D2	**C2**	Rh_2cap_4	**2-2**	14
D2	**C3**	Rh_2pfb_4	**2-3a**	13
			2-3b	1
D2	**C4**	Rh_2pfb_4	**2-4**	11
D2	**C5**	Rh_2cap_4	**2-5**	14
D2	**C6**	Rh_2cap_4	**2-6**	10
D2	**C7**	Rh_2piv_4	**2-7**	13[c]
D2	**C8**	Rh_2cap_4	**2-8**	13
D2	**C13**	Rh_2piv_4	**2-13**	12
D2	**C14**	Rh_2cap_4	**2-14**	10[d]
D2	**C15**	Rh_2cap_4	**2-15a**	11
			2-15b	1
D3	**C2**	Rh_2piv_4	**3-2**	13
D3	**C4**	Rh_2cap_4	**3-4a**	5[e]
			3-4b	5[e]
D4	**C1**	Rh_2pfb_4	**4-1**	56
D4	**C3**	Rh_2pfb_4	**4-3**	23
D4	**C5**	Rh_2cap_4	**4-5**	8
D4	**C13**	Rh_2piv_4	**4-13**	35
D4	**C17**	Rh_2pfb_4	**4-17**	11
D4	**C18**	Rh_2pfb_4	**4-18**	23
D5	**C1**	Rh_2pfb_4	**5-1**	26

[a]Reactions were performed in glass vials with an α-diazoamide substrate (20 µmol; limiting reactant), a co-substrate (5 equiv) and 1 mol % dirhodium catalyst. [b]Isolated yield of purified product. [c]dr: >95:<5. [d]dr: 51:49. [e]Obtained as a 50:50 mixture of inseparable products.

may stem from poor (co-)substrate solubility in some cases; and/or competitive O–H insertion into adventitious water.

On the basis of these results, additional reactions involving the α-diazoamide substrates **D4** (with a fluorosulfate warhead) and **D5** (with a sulfonyltriazole warhead) were also executed. In addition to using these two α-diazoamide substrates with different warheads, two additional co-substrates bearing an alkyne tag (**C17** and **C18**) were used. The reactions were assembled from stock solutions, with some variation in stock concentrations to improve solubility. After 24 h, the reaction products were analysed by LC–MS, and promising reactions selected for mass-directed purification. Seven additional intermolecular products were obtained (see Figure 3 and Table 2). The marked improvement in product yields, compared to those observed with **D1**–**3**, may reflect the change to the workflow, i.e., variation in stock concentration to improve solubility.

The diversity of the obtained products was increased by the multiple reaction modes of dirhodium carbenoids that were possible [14]. Overall, products were formed via O–H insertion into an alcohol (to give 14 products) or phenol (→ **2-4** and **3-4a**); N–H insertion into an indole (→ **1-3a**, **1-15b**, **2-3a**, **2-15b** and **4-3**), sulfonamide (→ **2-6**), aminopyrimidine (→ **2-13** and **4-13**) or amine (→ **4-18**); cyclopropanation (→ **2-7**); and formal C–H insertion into an indole (→ **1-15a** and **2-15a**) or naphthol (→ **2-4** and **3-4b**). In the case of **4** (2-naphthol) and **15** (5-methoxyindole), co-substrates containing functional groups with more than one potentially reactive site, two regioisomeric products were obtained. In the case of co-substrate **3**, which contains both an indole and an alcohol, thus raising chemoselectivity issues, products were observed from both O–H and N–H insertion. It is notable, however, that despite many of the co-substrates having multiple potentially reactive sites, one intermolecular reaction was generally dominant.
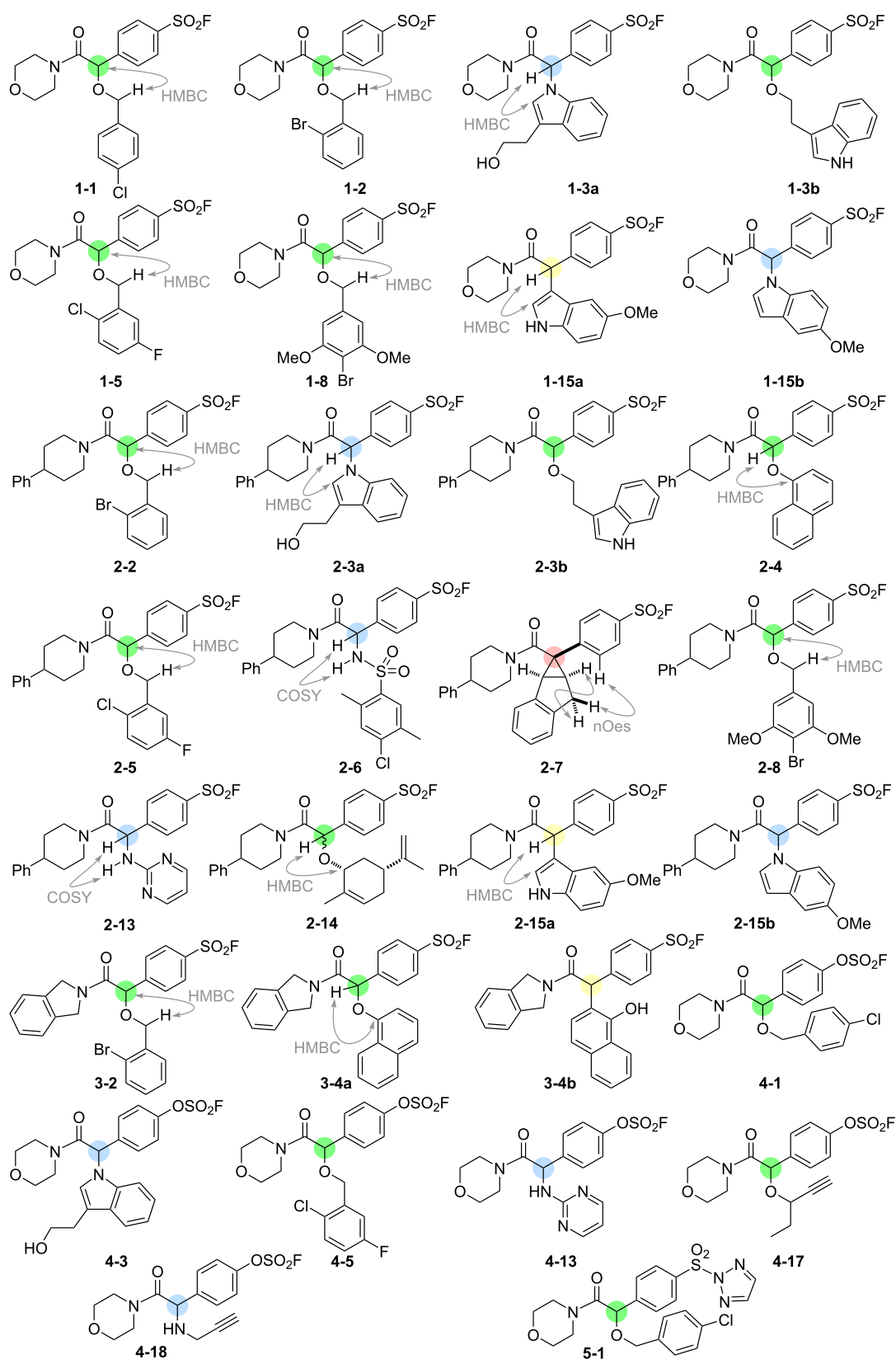
Figure 3: Structures and structure elucidation of intermolecular reaction products. The relevant reactivity modes are indicated by colour: O–H insertion (green); N–H insertion (blue); formal C–H insertion (yellow); and cyclopropanation (pink).

We have previously discovered sulfonyl fluoride probes with promising activity against *T. brucei,* a parasitic kinetoplastid that causes vector-borne African trypanosomiasis (sleeping sickness) [24]. We therefore screened the 23 sulfonyl fluoride probes (derived from diazo compounds **1**, **2** and **3**) against *T. brucei* in 96-well plate format (final concentrations: ≈2–50 μM). Four sulfonyl fluorides were found to have promising activity: **2-5** (EC_{50}: 9.38 ± 0.06 μM); **2-6** (EC_{50}: 6.81 ± 0.07 μM); **2-14** (EC_{50}: 9.26 ± 0.06 μM) and **2-15a** (EC_{50}: 11.9 ± 0.2 μM). It is notable that all of these active compounds are 4-phenylpiperidinyl amides derived from the same α-diazoamide **2**, suggesting that this feature is important for activity.

Conclusion

We have developed a connective synthesis of reactive probes bearing S(VI) electrophilic warheads. Each probe was prepared by rhodium-catalysed reaction between an α-diazo amide substrate bearing a warhead, and a co-substrate. The structural diversity of the probe set was increased by the multiple possible reaction modes of rhodium carbenoids, which enabled many different co-substrate classes and catalyst-driven selectivities to be exploited. A high-throughput synthetic approach was harnessed to identify substrate/co-substrate/catalyst combinations, which led to the productive formation of intermolecular reaction products. Overall, the approach enabled the synthesis of thirty diverse reactive probes. The probes were screened for activity against *T. brucei,* a parasitic kinetoplastid that causes vector-borne African trypanosomiasis, and four probes with promising anti-trypanosomal activity were identified. Remarkably, the synthetic approach was compatible with building blocks bearing three different S(VI) warheads, and enabled the direct connective synthesis of diverse reactive probes. We envisage that such probes may enable chemical modification of non-cysteine residues within proteins, and may be valuable in investigating and engineering the biology of proteins.

Supporting Information

Supporting Information File 1

Experimental part and NMR spectra of synthesised compounds.
[https://www.beilstein-journals.org/bjoc/content/supplementary/1860-5397-21-150-S1.pdf]

Acknowledgements

Funding

Author Contributions

Scott Rice: conceptualization; data curation; investigation; methodology; writing – review & editing. Julian Chesti: data curation; investigation; methodology; writing – review & editing. William R. T. Mosedale: data curation; investigation; methodology; writing – review & editing. Megan H. Wright: funding acquisition; supervision; writing – review & editing. Stephen P. Marsden: funding acquisition; supervision; writing – review & editing. Terry K. Smith: funding acquisition; supervision; writing – review & editing. Adam Nelson: conceptualization; funding acquisition; supervision; writing – original draft.

ORCID® iDs

Julian Chesti - https://orcid.org/0000-0001-5416-7648
Megan H. Wright - https://orcid.org/0000-0003-2731-4707
Stephen P. Marsden - https://orcid.org/0000-0002-2723-8954
Adam Nelson - https://orcid.org/0000-0003-3886-363X

Data Availability Statement

All data that supports the findings of this study is available in the published article and/or the supporting information of this article.

References

1. Drewes, G.; Knapp, S. *Trends Biotechnol.* **2018,** *36,* 1275–1286. doi:10.1016/j.tibtech.2018.06.008
2. Boike, L.; Henning, N. J.; Nomura, D. K. *Nat. Rev. Drug Discovery* **2022,** *21,* 881–898. doi:10.1038/s41573-022-00542-z
3. Lu, W.; Kostic, M.; Zhang, T.; Che, J.; Patricelli, M. P.; Jones, L. H.; Chouchani, E. T.; Gray, N. S. *RSC Chem. Biol.* **2021,** *2,* 354–367. doi:10.1039/d0cb00222d
4. Crowley, V. M.; Thielert, M.; Cravatt, B. F. *ACS Cent. Sci.* **2021,** *7,* 613–623. doi:10.1021/acscentsci.0c01336
5. Douangamath, A.; Fearon, D.; Gehrtz, P.; Krojer, T.; Lukacik, P.; Owen, C. D.; Resnick, E.; Strain-Damerell, C.; Aimon, A.; Ábrányi-Balogh, P.; Brandão-Neto, J.; Carbery, A.; Davison, G.; Dias, A.; Downes, T. D.; Dunnett, L.; Fairhead, M.; Firth, J. D.; Jones, S. P.; Keeley, A.; Keserü, G. M.; Klein, H. F.; Martin, M. P.; Noble, M. E. M.; O'Brien, P.; Powell, A.; Reddi, R. N.; Skyner, R.; Snee, M.; Waring, M. J.; Wild, C.; London, N.; von Delft, F.; Walsh, M. A. *Nat. Commun.* **2020,** *11,* 5047. doi:10.1038/s41467-020-18709-w

6. Resnick, E.; Bradley, A.; Gan, J.; Douangamath, A.; Krojer, T.; Sethi, R.; Geurink, P. P.; Aimon, A.; Amitai, G.; Bellini, D.; Bennett, J.; Fairhead, M.; Fedorov, O.; Gabizon, R.; Gan, J.; Guo, J.; Plotnikov, A.; Reznik, N.; Ruda, G. F.; Díaz-Sáez, L.; Straub, V. M.; Szommer, T.; Velupillai, S.; Zaidman, D.; Zhang, Y.; Coker, A. R.; Dowson, C. G.; Barr, H. M.; Wang, C.; Huber, K. V. M.; Brennan, P. E.; Ovaa, H.; von Delft, F.; London, N. *J. Am. Chem. Soc.* **2019,** *141,* 8951–8968. doi:10.1021/jacs.9b02822

7. St. Denis, J. D.; Chessari, G.; Cleasby, A.; Cons, B. D.; Cowan, S.; Dalton, S. E.; East, C.; Murray, C. W.; O'Reilly, M.; Peakman, T.; Rapti, M.; Stow, J. L. *J. Med. Chem.* **2022,** *65,* 12319–12333. doi:10.1021/acs.jmedchem.2c01044

8. Brulet, J. W.; Borne, A. L.; Yuan, K.; Libby, A. H.; Hsu, K.-L. *J. Am. Chem. Soc.* **2020,** *142,* 8270–8280. doi:10.1021/jacs.0c00648

9. Gilbert, K. E.; Vuorinen, A.; Aatkar, A.; Pogány, P.; Pettinger, J.; Grant, E. K.; Kirkpatrick, J. M.; Rittinger, K.; House, D.; Burley, G. A.; Bush, J. T. *ACS Chem. Biol.* **2023,** *18,* 285–295. doi:10.1021/acschembio.2c00633

10. Huang, T.; Hosseinibarkooie, S.; Borne, A. L.; Granade, M. E.; Brulet, J. W.; Harris, T. E.; Ferris, H. A.; Hsu, K.-L. *Chem. Sci.* **2021,** *12,* 3295–3307. doi:10.1039/d0sc06623k

11. Boström, J.; Brown, D. G.; Young, R. J.; Keserü, G. M. *Nat. Rev. Drug Discovery* **2018,** *17,* 709–727. doi:10.1038/nrd.2018.116

12. Zanon, P. R. A.; Yu, F.; Musacchio, P.; Lewald, L.; Zollo, M.; Krauskopf, K.; Mrdović, D.; Raunft, P.; Maher, T. E.; Cigler, M.; Chang, C.; Lang, K.; Toste, F. D.; Nesvizhskii, A. I.; Hacker, S. M. *ChemRxiv* **2021.** doi:10.26434/chemrxiv-2021-w7rss-v2

13. Narayanan, A.; Jones, L. H. *Chem. Sci.* **2015,** *6,* 2650–2659. doi:10.1039/c5sc00408j

14. Doraghi, F.; Baghershahi, P.; Ghasemi, M.; Mahdavi, M.; Al-Harrasi, A. *RSC Adv.* **2024,** *14,* 39337–39352. doi:10.1039/d4ra07010k See for a review.

15. Chow, S.; Green, A. I.; Arter, C.; Liver, S.; Leggott, A.; Trask, L.; Karageorgis, G.; Warriner, S.; Nelson, A. *Synthesis* **2020,** *52,* 1695–1706. doi:10.1055/s-0039-1690905

16. Peng, C.; Cheng, J.; Wang, J. *J. Am. Chem. Soc.* **2007,** *129,* 8708–8709. doi:10.1021/ja073010+

17. Ye, F.; Qu, S.; Zhou, L.; Peng, C.; Wang, C.; Cheng, J.; Hossain, M. L.; Liu, Y.; Zhang, Y.; Wang, Z.-X.; Wang, J. *J. Am. Chem. Soc.* **2015,** *137,* 4435–4444. doi:10.1021/ja513275c

18. Yamamoto, K.; Qureshi, Z.; Tsoung, J.; Pisella, G.; Lautens, M. *Org. Lett.* **2016,** *18,* 4954–4957. doi:10.1021/acs.orglett.6b02423

19. Fu, L.; Mighion, J. D.; Voight, E. A.; Davies, H. M. L. *Chem. – Eur. J.* **2017,** *23,* 3272–3275. doi:10.1002/chem.201700101

20. Moody, C. J.; Doyle, K. J. *Prog. Heterocycl. Chem.* **1997,** *9,* 1–16. doi:10.1016/s0959-6380(97)80003-7

21. Green, A. I.; Tinworth, C. P.; Warriner, S.; Nelson, A.; Fey, N. *Chem. – Eur. J.* **2021,** *27,* 2402–2409. doi:10.1002/chem.202003801

22. Squibb, A. W.; Taylor, M. R.; Parnas, B. L.; Williams, G.; Girdler, R.; Waghorn, P.; Wright, A. G.; Pullen, F. S. *J. Chromatogr. A* **2008,** *1189,* 101–108. doi:10.1016/j.chroma.2007.11.017

23. Griggs, S. D.; Piticari, A.-S.; Liver, S.; Arter, C.; Sievers, S.; Marsden, S. P.; Nelson, A. *Chem. Commun.* **2025,** *61,* 3528–3531. doi:10.1039/d4cc06605g

24. Mantilla, B. S.; White, J. S.; Mosedale, W. R. T.; Gomm, A.; Nelson, A.; Smith, T. K.; Wright, M. H. *Commun. Chem.* **2024,** *7,* 237. doi:10.1038/s42004-024-01327-8

BEILSTEIN JOURNAL OF ORGANIC CHEMISTRY

Efficient solid-phase synthesis and structural characterization of segetalins A–H, J and K

Liangyu Liu, Wanqiu Lu, Quanping Guo[*] and Zhaoqing Xu[*]

Abstract

This study establishes an efficient solid-phase strategy for the total synthesis of segetalins A–H, J and K (**1–10**), bioactive cyclopeptides isolated from *Vaccaria segetalis*. Linear precursors were assembled on cost-effective 2-chlorotrityl chloride resin via Fmoc-SPPS, followed by PyBOP-mediated head-to-tail cyclization in DMF (10^{-3} M). After RP-HPLC purification, all cyclopeptides were obtained in 45–70% isolated yields. Structural identities were confirmed by HRESIMS, NMR, and HPLC (>95% purity). Circular dichroism (CD) spectroscopy revealed distinct secondary structures, including β-sheets (**1**, **2**, **3**, **4**, **7**, **8**, **10**) and α-helical elements (**5**, **6**). This scalable methodology overcomes limitations of prior syntheses, enabling biological evaluation.

Introduction

Cyclopeptides have garnered significant research interest owing to their unique conformational constraints imposed by cyclization and diverse biological activities [1-3]. Specifically, plant-derived cyclopeptides represent a valuable source of potential lead compounds for drug discovery [4]. Segetalins A–H, J and K (**1–10**), isolated from the seeds of *Vaccaria segetalis* (Caryophyllaceae), are head-to-tail cyclic oligopeptides comprising 5–9 amino acid residues [5-13]. These natural products exhibit a significant diversity of pharmacological activities [14-16], including estrogen-like activity (**1**, **2**, **7**, **8**), antitumor effects (**5**), and antimicrobial properties (**3**). Given their unique structural features and pharmacological potential, segetalins have become important targets for both synthetic chemistry and

drug development. However, efficient and general synthetic routes to access this family have remained limited over the past decades.

Previous synthetic approaches have encountered significant challenges. Sonnet et al. reported the first total synthesis of segetalin A (**1**) via Sasrin resin-based SPPS, followed by cyclization under highly dilute conditions (10^{-4} M) with diphenylphosphoryl azide (DPPA) [17]. While successful, this approach suffers from the high cost of the specialized resin and large solvent volumes required for dilution, coupled with DPPA's poor efficiency in forming sterically hindered peptide bonds involving residues like Val or Ile. Dahiya and Kaur synthesized sege-

talin C (**3**) via a solution-phase fragment coupling strategy, culminating in cyclization mediated by *N*,*N*'-dicyclohexylcarbodiimide (DCC)/*N*-methylmorpholine (NMM) at 0 °C for 7 days [18]. This method, however, is lengthy, operationally complex, difficult for product isolation, and carries a significant risk of racemization. Wong and Jolliffe synthesized segetalins B (**2**) and G (**7**) using a pseudoprolinic acid strategy to induce *cis*-amide bond formation, followed by desulfurization [19]. Despite achieving cyclization, this route involves intricate procedures, expensive starting materials, and has limited applicability to other segetalins.

Given the limitations of existing methodologies and the biological significance of the segetalins, we sought to develop an efficient, scalable, and generally applicable solid-phase synthesis strategy for the *Vaccaria segetalis* cyclopeptide family.

Results and Discussion
Synthesis strategy and optimization

While both solution-phase and solid-phase approaches are viable for peptide synthesis, Fmoc-based SPPS offers distinct advantages in operational simplicity and efficiency for laboratory-scale production [20]. We therefore devised a streamlined solid-phase strategy for synthesizing the *Vaccaria segetalis* cyclopeptide family (Scheme 1).

Building upon previous work [17-19], we focused on optimizing key parameters: resin selection, Fmoc deprotection conditions, coupling reagents for linear assembly, and crucially, the cyclization step. Cost-effectiveness and commercial availability led us to select 2-chlorotrityl chloride resin as the solid support, enabling mild cleavage of the partially protected linear peptide precursor [21]. Efficient Fmoc deprotection was achieved using a solution of 1% pyridine and 1% 1,8-diazabicyclo[5.4.0]undec-7-ene (DBU) in *N*,*N*-dimethylformamide (DMF) [22]. For the
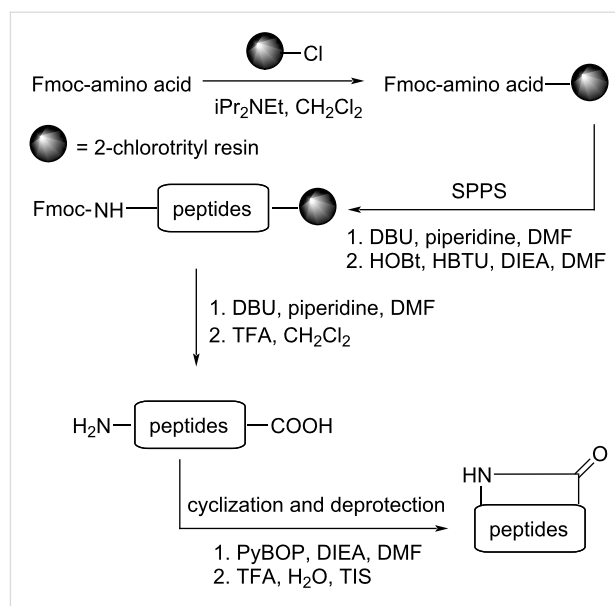
Scheme 1: Preparation of segetalins A–H, J and K.

assembly of the linear sequences, coupling efficiency was significantly enhanced using a 1:1 mixture of 1-hydroxybenzotriazole (HOBt) and 2-(1*H*-benzotriazol-1-yl)-1,1,3,3-tetramethyl-uronium hexafluorophosphate (HBTU) in DMF [23]. Finally, we obtained crude linear peptides with 75% to 95% yields (Table 1).

The critical head-to-tail cyclization step proved challenging. Initial attempts using common coupling reagents such as 1-[bis(dimethylamino)methylene]-1*H*-1,2,3-triazolo[4,5-*b*]pyridinium 3-oxide hexafluorophosphate (HATU), HBTU, or HOBt alone in DMF failed to produce any detectable cyclized product [24-26]. Ultimately, successful macrocyclization was achieved by employing benzotriazol-1-yloxytripyrrolidinophosphonium hexafluorophosphate (PyBOP) as the coupling reagent in DMF

Table 1: Preparation of linear peptides for segetalins A–H, J and K.

	Structure	Yield[a]
1	Gly-Val-Pro-Val-Trp(Boc)-Ala	89%
2	Gly-Val-Ala-Trp(Boc)-Ala	77%
3	Gly-Leu-His(Trt)-Phe-Ala-Phe-Pro	93%
4	Gly-Leu-Ser(*t*-Bu)-Phe-Ala-Phe-Pro	91%
5	Gly-Tyr(*t*-Bu)-Val-Pro-Leu-Trp(Boc)-Pro	89%
6	Ala-Ser(*t*-Bu)-Tyr(*t*-Bu)-Ser(*t*-Bu)-Ser(*t*-Bu)-Lys(Boc)-Pro-Phe-Ser(*t*-Bu)	87%
7	Gly-Val-Lys(Boc)-Tyr(*t*-Bu)-Ala	95%
8	Gly-Tyr(*t*-Bu)-Arg(Pbf)-Phe-Ser(*t*-Bu)	94%
9	Phe-Gly-Thr(*t*-Bu)-His(Trt)-Gly-Leu-Pro-Ala-Pro	89%
10	Gly-Arg(Pbf)-Val-Lys(Boc)-Ala	87%

[a]Yield of crude linear peptide.

at a concentration of 10^{-3} M. After cleavage from the resin and global side-chain deprotection, the crude cyclic peptides were purified by preparative RP-HPLC. This optimized protocol afforded segetalins A–H, J and K (**1**–**10**) with 45% to 70% isolated yields (Figure 1).

Structural characterization

The synthetic compounds **1**–**10** were rigorously characterized to confirm their identity and purity (see Supporting Information

File 1). High-resolution electrospray ionization mass spectrometry (HRESIMS) data for all compounds matched the calculated exact masses for their respective molecular formulas. NMR spectroscopic analysis in appropriate deuterated solvents (e.g., DMSO-d_6, D_2O) fully corroborated the amino acid sequence and cyclic connectivity, demonstrating unequivocal structural identity with the natural isolates. Analytical HPLC confirmed the high purity (>95%) of all synthetic segetalins. However, experimental data for segetalin C revealed the exis-
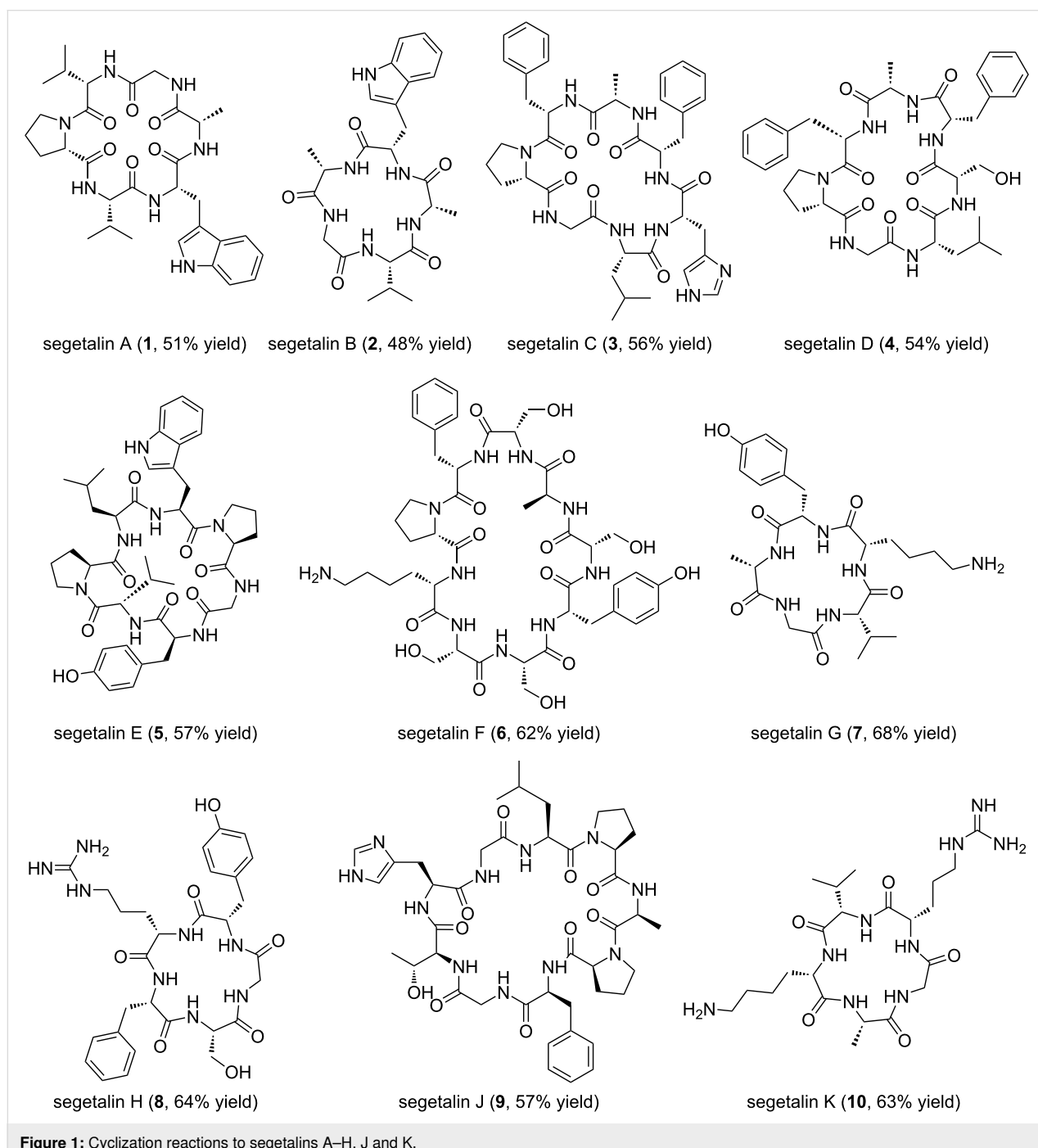

Figure 1: Cyclization reactions to segetalins A–H, J and K.

tence of a multi-state conformational equilibrium in solution, which is dependent on solvent polarity.

Secondary structure analysis by circular dichroism (CD)

The secondary structures of compounds **1**–**10** were investigated using circular dichroism (CD) spectroscopy in aqueous buffer (0.01×PBS), deionized H_2O, and 30% TFE (2,2,2-trifluoro-ethanol) (Figure 2). CD spectra in the far-UV region (190–250 nm) provide signatures of peptide backbone conformation [27-29]: a random coil typically shows a negative band near 198 nm and a positive band near 218 nm; an α-helix exhibits characteristic minima at 208 nm and 222 nm and a maximum near 192 nm; β-sheet structures are often indicated
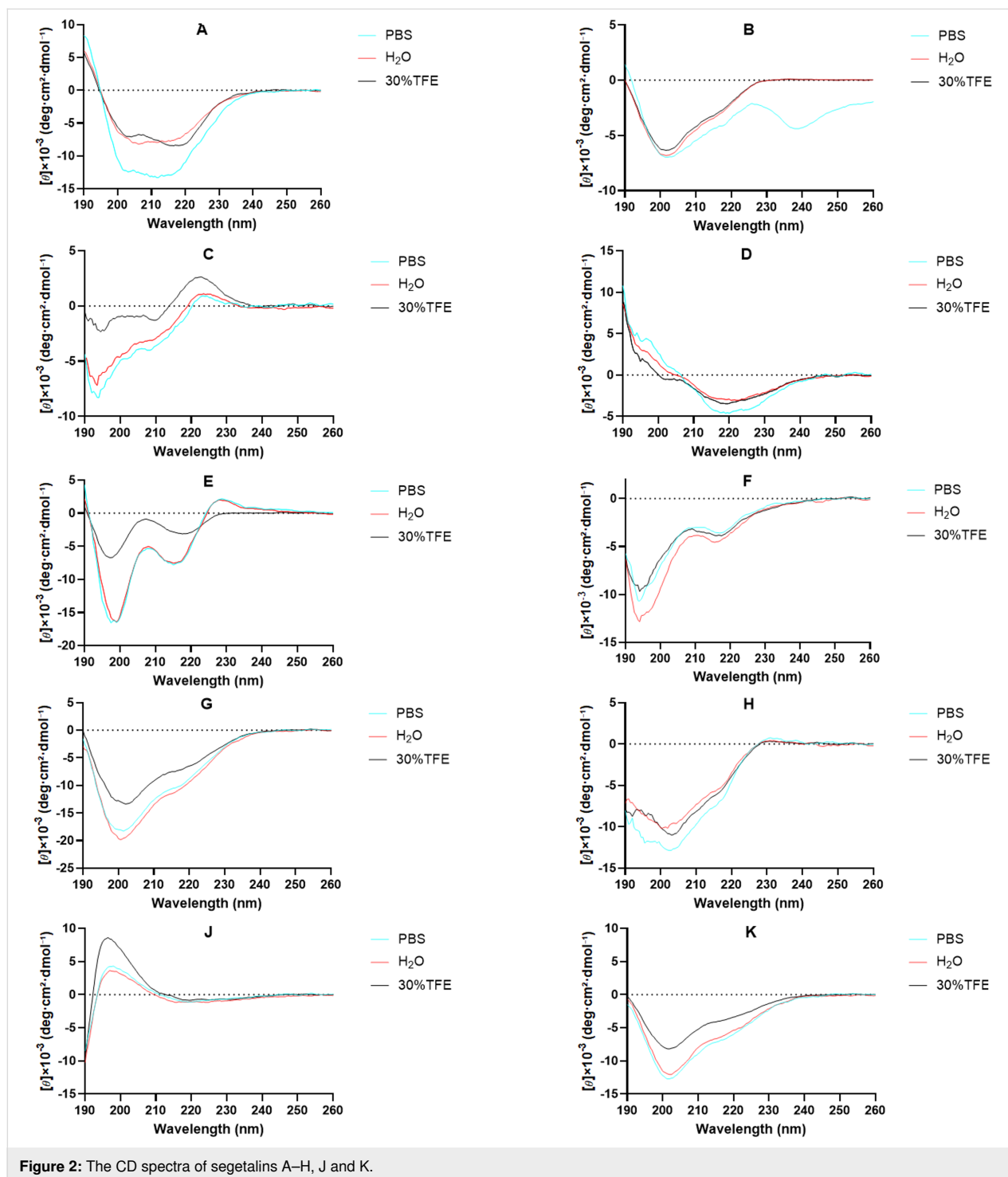

Figure 2: The CD spectra of segetalins A–H, J and K.

by a single minimum between 210–220 nm and a maximum below 200 nm.

CD spectroscopy revealed that cyclic topology shifts characteristic peaks and stabilizes secondary structures through cooperative ring size/sequence/solvent effects [30]. TFE disrupts the hydrogen-bonding network of water, reduces solvent polarity, and enhances the stability of intramolecular hydrogen bonds in the peptide backbone, thereby promoting the formation of stable secondary structures (such as α-helices or β-sheets) in cyclic peptides. Spectra acquired in H_2O, 0.01×PBS, and 30% TFE (Table S1, Supporting Information File 1) demonstrate: (i) definitive β-sheet signatures (217 nm minima) in **1**, **3**, **4**; (ii) enhanced β-sheet stability from constrained macrocycles in **2**, **7**, **8**, **10**; (iii) universal α-helix induction by TFE in **1–10**, with **5** and **6** retaining helicity in aqueous buffers.

Conclusion

We have developed an efficient and reliable solid-phase synthesis strategy for the cyclopeptide family of segetalins A–H, J and K from *Vaccaria segetalis*. Key optimizations include the use of a cost-effective 2-chlorotrityl chloride resin, efficient Fmoc deprotection and linear coupling conditions (HOBt/HBTU), and the identification of PyBOP as a highly effective coupling reagent for the challenging head-to-tail macrocyclization step under moderate dilution (10^{-3} M). This protocol afforded the target cyclic peptides in practical isolated yields (45–70%) and high purity. Comprehensive structural characterization by HRESIMS, NMR, and HPLC confirmed the identity and high purity of the synthetic segetalins. CD spectroscopy provided insights into their secondary structural preferences. This robust and scalable methodology overcomes significant limitations of previous synthetic approaches, providing ample quantities of these bioactive cyclopeptides for detailed biological evaluation and structure–activity relationship studies. The systematic investigation of the their key biological activities, including estrogenic activity (assessed via breast cell proliferation assays), antitumor activity (evaluated through HeLa cell inhibition assays), and antibacterial activity (evaluated against Gram-positive bacteria), will be conducted in our laboratory.

Supporting Information

Supporting Information File 1
Experimental section, characterization and copies of spectra.
[https://www.beilstein-journals.org/bjoc/content/supplementary/1860-5397-21-202-S1.pdf]

Author Contributions

Liangyu Liu: investigation; methodology; writing – original draft. Wanqiu Lu: investigation; methodology. Quanping Guo: writing – original draft. Zhaoqing Xu: conceptualization; funding acquisition; project administration; supervision; writing – original draft.

ORCID® iDs

Zhaoqing Xu - https://orcid.org/0000-0001-7663-6249

Data Availability Statement

All data that supports the findings of this study is available in the published article and/or the supporting information of this article.

References

1. Ji, X.; Nielsen, A. L.; Heinis, C. *Angew. Chem., Int. Ed.* **2024,** *63,* e202308251. doi:10.1002/anie.202308251
2. Jin, K. *Future Med. Chem.* **2020,** *12,* 1687–1690. doi:10.4155/fmc-2020-0171
3. Nielsen, D. S.; Shepherd, N. E.; Xu, W.; Lucke, A. J.; Stoermer, M. J.; Fairlie, D. P. *Chem. Rev.* **2017,** *117,* 8094–8128. doi:10.1021/acs.chemrev.6b00838
4. Zhang, J.; Yuan, J.; Li, Z.; Fu, C.; Xu, M.; Yang, J.; Jiang, X.; Zhou, B.; Ye, X.; Xu, C. *Med. Res. Rev.* **2021,** *41,* 3096–3117. doi:10.1002/med.21792
5. Condie, J. A.; Nowak, G.; Reed, D. W.; Balsevich, J. J.; Reaney, M. J. T.; Arnison, P. G.; Covello, P. S. *Plant J.* **2011,** *67,* 682–690. doi:10.1111/j.1365-313x.2011.04626.x
6. Morita, H.; Sook Yun, Y.; Takeya, K.; Itokawa, H.; Shiro, M. *Tetrahedron* **1995,** *51,* 5987–6002. doi:10.1016/0040-4020(95)00277-f
7. Morita, H.; Yun, Y. S.; Takeya, K.; Itokawa, H.; Shirota, O. *Phytochemistry* **1996,** *42,* 439–441. doi:10.1016/0031-9422(95)00911-6
8. Yun, Y. S.; Morita, H.; Takeya, K.; Itokawa, H. *J. Nat. Prod.* **1997,** *60,* 216–218. doi:10.1021/np960617n
9. Morita, H.; Yun, Y. S.; Takeya, K.; Itokawa, H. *Tetrahedron Lett.* **1994,** *35,* 9593–9596. doi:10.1016/0040-4039(94)88519-2
10. Itokawa, H.; Yun, Y.; Morita, H.; Takeya, K.; Yamada, K. *Planta Med.* **1995,** *61,* 561–562. doi:10.1055/s-2006-959373
11. Morita, H.; Yun, Y. S.; Takeya, K.; Itokawa, H.; Yamada, K. *Tetrahedron* **1995,** *51,* 6003–6014. doi:10.1016/0040-4020(95)00278-g
12. Morita, H.; Eda, M.; Iizuka, T.; Hirasawa, Y.; Sekiguchi, M.; Yun, Y. S.; Itokawa, H.; Takeya, K. *Bioorg. Med. Chem. Lett.* **2006,** *16,* 4458–4461. doi:10.1016/j.bmcl.2006.06.083
13. Barber, C. J. S.; Pujara, P. T.; Reed, D. W.; Chiwocha, S.; Zhang, H.; Covello, P. S. *J. Biol. Chem.* **2013,** *288,* 12500–12510. doi:10.1074/jbc.m112.437947
14. Houshdar Tehrani, M. H.; Gholibeikian, M.; Bamoniri, A.; Mirjalili, B. B. F. *Front. Endocrinol.* **2021,** *11,* 600856. doi:10.3389/fendo.2020.600856

15. Dahiya, R.; Dahiya, S.; Shrivastava, J.; Fuloria, N. K.; Gautam, H.; Mourya, R.; Fuloria, S. *Arch. Pharm. (Weinheim, Ger.)* **2021,** *354,* 2000446. doi:10.1002/ardp.202000446

16. Tian, M.; Huang, Y.; Wang, X.; Cao, M.; Zhao, Z.; Chen, T.; Yuan, C.; Wang, N.; Zhang, B.; Li, C.; Zhou, X. *Front. Chem. (Lausanne, Switz.)* **2021,** *9,* 666280. doi:10.3389/fchem.2021.666280

17. Sonnet, P.; Petit, L.; Marty, D.; Guillon, J.; Rochette, J.; Brion, J.-D. *Tetrahedron Lett.* **2001,** *42,* 1681–1683. doi:10.1016/s0040-4039(00)02354-6

18. Dahiya, R.; Kaur, K. *Arzneim. Forsch.* **2008,** *58,* 29–34. doi:10.1055/s-0031-1296463

19. Wong, M. S. Y.; Jolliffe, K. A. *Pept. Sci.* **2018,** *110,* e24042. doi:10.1002/pep2.24042

20. Behrendt, R.; White, P.; Offer, J. *J. Pept. Sci.* **2016,** *22,* 4–27. doi:10.1002/psc.2836

21. In this study, solid-phase synthesis was accomplished using the cost-effective dichlorotrityl chloride (DCL) resin. Its commercial price is approximately $2.1 per gram (from suppliers such as Shanghai Acmec Biochemical Technology Co., Ltd), and it is readily available in multi-kilogram quantities. This price stands in sharp contrast to other resins commonly used in analogous syntheses: for instance, Wang resin and Sasrin resin are priced at about $100 per gram and these resins are not available in kilogram quantities (BACHEM). The significant cost advantage of DCL resin makes it an economically viable option for large-scale combinatorial library synthesis and industrial applications.

22. Wang, M.; Pan, D.; Zhang, Q.; Lei, Y.; Wang, C.; Jia, H.; Mou, L.; Miao, X.; Ren, X.; Xu, Z. *J. Am. Chem. Soc.* **2024,** *146,* 6675–6685. doi:10.1021/jacs.3c12879

23. Qi, R.; Chen, Q.; Liu, L.; Ma, Z.; Pan, D.; Wang, H.; Li, Z.; Wang, C.; Xu, Z. *Nat. Commun.* **2023,** *14,* 3295. doi:10.1038/s41467-023-38871-1

24. White, C. J.; Yudin, A. K. *Nat. Chem.* **2011,** *3,* 509–524. doi:10.1038/nchem.1062

25. Fagundez, C.; Sellanes, D.; Serra, G. *ACS Comb. Sci.* **2018,** *20,* 212–219. doi:10.1021/acscombsci.7b00154

26. Ma, B.; Litvinov, D. N.; He, L.; Banerjee, B.; Castle, S. L. *Angew. Chem., Int. Ed.* **2009,** *48,* 6104–6107. doi:10.1002/anie.200902425

27. Ranjbar, B.; Gill, P. *Chem. Biol. Drug Des.* **2009,** *74,* 101–120. doi:10.1111/j.1747-0285.2009.00847.x

28. Kuril, A. K.; Vashi, A.; Subbappa, P. K. *J. Pept. Sci.* **2025,** *31,* e3648. doi:10.1002/psc.3648

29. Fiametti, L. O.; Franco, C. A.; Nunes, L. O. C.; de Castro, L. M.; Santos-Filho, N. A. *Int. J. Mol. Sci.* **2025,** *26,* 2017. doi:10.3390/ijms26052017

30. Chan, L. Y.; Zhang, V. M.; Huang, Y.-h.; Waters, N. C.; Bansal, P. S.; Craik, D. J.; Daly, N. L. *ChemBioChem* **2013,** *14,* 617–624. doi:10.1002/cbic.201300034